

# Load-Displacement Curves of Spot Welded, Bonded, and Weld-Bonded Joints for Dissimilar Materials and Thickness

E.A. Al-Bahkali

Department of Mechanical Engineering, College of Engineering, King Saud University, P.O. Box 800, Riyadh 11421, Saudi Arabia

Received 15 April 2011; accepted 21 September 2011

منحنيات الحمل والاستطالة لمعادن مختلفة النوع والسماعة مرتبطة بواسطة لحام النقطة مختلفة المواد والسماعة  
ع. أ. البهكلي

**الخلاصة:** يقوم هذا البحث على بناء نماذج ثلاثية الأبعاد لقطعيتين ملتحمتين بواسطة لحام النقطة، وبمواد اللصق، و بالاثنتين معا بطريقة العناصر المحددة باستخدام برنامج أباكس. كل نموذج يتكون من قطعيتين مختلفتين في النوع والسماعة وملتحمتين مع بعضهما البعض ويتعرضا لقوة شد. وفي النماذج التي تحتوي على لحام بواسطة الطبقة اللاصقة فقد تم استخدام سمك ثابت لتلك الطبقة. وقد تم استخدام التجارب العملية للحصول على خواص المواد بالتفصيل مثل تعريف منطقة المرونة و اللدونة، ومعامل المرونة، وخواص منطقة لحام النقطة والمنطقة المتأثرة حولها بالحرارة، ومنطقة المعدن الأساس. كما تم استخدام عملية التثليم (إحداث فجوة في المادة) لتحديد حد التشقق. وقد تم الحصول على منحنى الحمل والاستطالة لجميع النماذج ومقارنتها مع بعضها البعض للحصول على أفضل طريقة لوصل المعادن المختلفة.

**المفردات المفتاحية:** لحام النقطة، المادة اللاصقة، لحام النقطة مع المادة اللاصقة، النمذجة باستخدام العناصر المحددة، مادة مختلفة

**Abstract:** Three-dimensional finite element models of spot welded, bonded and weld-bonded joints are developed using ABAQUS software. Each model consists of two strips with dissimilar materials and thickness and is subjected to an axial loading. The bonded and weld-bonded joints have specific adhesive thickness. A detailed experimental plan to define many properties and quantities such as, the elastic - plastic properties, modulus of elasticity, fracture limit, and properties of the nugget and heat affected zones are carried out. Experiments include standard testing of the base metal, the adhesive, the nugget and heat affected zone. They also include employing the indentation techniques, and ductile fracture limits criteria, using the special notch tests. Complete load-displacement curves are obtained for all joining models and a comparison is made to determine the best combination.

**Keywords:** Spot welding, Adhesive, Weld-bonded, Finite element modelling, Dissimilar material

## 1. Introduction

Resistance Spot Welding (RSW) has been used for decades as a joining method for sheet metal. Weld-bonded is a combination of resistance spot welding and adhesive bonding, which has gathered wide acceptance as an effective joining method for significant enhancement of static, dynamic and impact resistance of the joint. It also improves the corrosion and noise resistance as well as stiffness of the joint, com-

pared to those observed in case of conventional resistance spot welding. Industrial applications such as automobile and aerospace are good examples of using weld-bonded process.

In order to reach an optimum welding quality of a spot welded or a weld-bonded joints, different calibration trials must be conducted to setup the optimum welding parameters, *i.e.* welding current, electrode force, and welding time (Bouyouf *et al.* 2007, Farukawa *et al.* 2006).

\*Corresponding author e-mail: ebahkali@ksu.edu.sa

Various techniques have been used to analyze the spot welded and weld-bonded joints. Finite element method (FEM) is one of these techniques, which has received a wide acceptance among researchers as a tool for modelling and analysis of welding joints. It has the capability to predict stress distribution, stress concentration, and failure modes for both weld-bonded and spot welded nuggets. To model real joint connection using FE, the elastic and plastic mechanical properties of the parts must be taken into consideration. Therefore, many researchers worked on weld-bonded technology experimentally and numerically in an attempt to represent real joint connection. Kang *et al.* (2006) used Tabor-equation to transform the indentation data to true stress-strain values. More sophisticated methods to determine the elastic-plastic properties from indentation are used and reported by (Venkatesh *et al.* 2000 and Dao *et al.* 2001). They used instrumented sharp indentation machine, where the load and displacement during indentation were recorded continuously. Li *et al.* (2005) studied numerically the deformation and fracture initiation of mode I (normal strength and toughness) in adhesive bonding. Later, Yang *et al.* (2001) investigated the fracture toughness data for adhesive. In addition, (Li *et al.* 2006) continued the study of the mixed mode cohesive-zone models for fracture of an adhesively bonded polymer-matrix composite. In their work, the load displacement curve of single lap shear joint obtained by FE analysis showed an acceptable agreement with the experimental data. Moreover, (Cavalli *et al.* 2004) investigated the finite element model based on cohesive element model for weld-bonded joint of AA-5754 Aluminium alloy.

It is also important to study the microstructure and mechanical properties at the nugget and the heat affected zone (HAZ) caused by welding process because the plastic properties of the nugget and HAZ are different from the base metal. Kong *et al.* (2008) reported that, the elastic-plastic properties have to be defined for each region of spot welded joint, by the combination of indentation and extensive FE simulation of the indentation. Al-Bahkali *et al.* (2010) have developed a 3D FE model of spot welded, adhesive bonded, and weld bonded joints of austenitic stainless steel sheets of 1.0 mm thickness. Their models are based on elastic-plastic properties, and ductile fracture limit criteria for steel, whereas the adhesive bonding is modelled based on traction separation. They have also studied the elastic - plastic properties, modulus of elasticity, fracture limit, nugget and HAZ properties. The load-displacement curves obtained from the FE models are in agreement with the experimental data.

Spot weld and weld-bonding of dissimilar materials are of interest to engineers and scientists for efficiently joining two different materials. Hasanbasoglu

and Kacar (2007) investigated the influence of the primary welding parameters on the morphology, micro-hardness, and shear tensile load bearing capacity of two dissimilar steel welds. Darwish (2004) analyzed spot-welded and weld-bonded of dissimilar material joints using FEM. He showed that the stresses were more concentrated towards the member that had the lowest melting point of the joint. He pointed that, adding an adhesive layer in combination with the spot weld resulted in eliminating the stress concentration and strength ending dissimilar material joints.

The aim of present work is to study the load-displacement curves toward the best combination for spot weld, bonded, and weld-bonded for dissimilar materials and thicknesses. 3D FE models are developed for dissimilar spot welded, bonded, and bond-welded joints, based on elastic-plastic properties and ductile fracture limit criteria for each region (base metal, nugget and HAZ). These developed FE models can predict the deformation and fracture initiation, including the maximum load of the weld-bonded joint as well as spot welded and adhesive bonded for any combination of sheet thickness, overlap area, and nugget diameter. In the FE models, the plastic properties of each welding region are defined by spherical indentation and transformed to true stress-true strain using Ahn-equation 2006. Furthermore, the ductile fracture limit criteria are employed to determine the fracture initiation point in the FE model (Bao 2005; Mackenzie *et al.* 1977; Hancock, Mackenzie 1976). This method is based on evaluating the stress triaxiality versus equivalent plastic strain conditions. The fracture limits of adhesive bonding are introduced in terms of maximum normal stress and shear stress of traction separation, which is defined experimentally (Sun *et al.* 2009, Diehl 2005).

## 2. Finite Element Model

### 2.1 Geometry

In this section, three different finite elements models are considered. These models are a single lap bonded model, a single lap spot weld model, and a single lap weld-bonded model. Figure 1 shows the front view (F.V) and top view (T.V) configurations, dimensions, constraints and loading conditions for bonded and weld-bonded models. Spot weld model is similar to weld-bonded except that it does not have an adhesive layer around the nugget. The total length of each model is 175 mm. The strips thicknesses are 1 mm and 1.5 mm, respectively.

The following assumptions are considered throughout the idealization process. The models are three-dimensional and because of symmetry half of the model is considered to save computation time. The

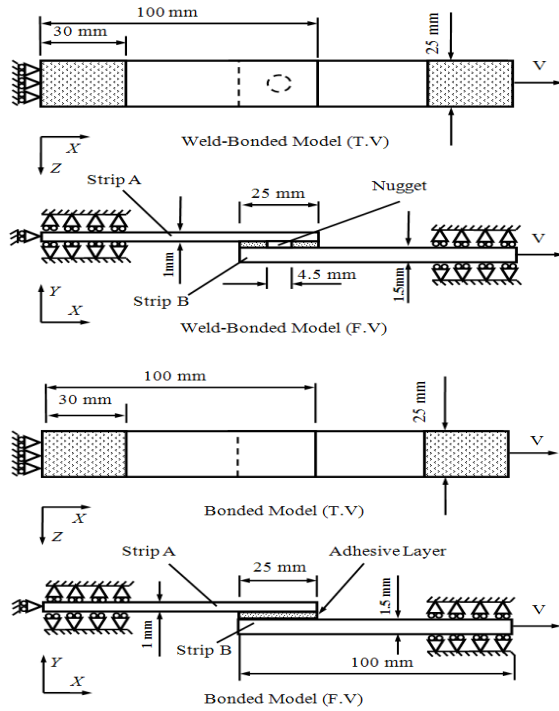


Figure 1. Bonded and weld-bonded models

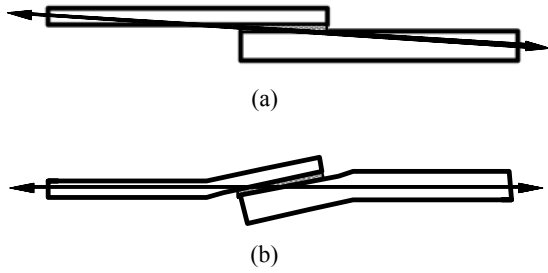


Figure 2. Lap-joint have (a) a line of action is not initially parallel to the adhesive layer, (b) the overlap area bends as load increases

adhesive layer is isotropic and has a thickness of 0.12 mm. There is no adhesive layer in a zone 1 mm around the circumference of the weld nugget and the depth of the indentation is assumed to be 0.1 mm for both strips (Baohua *et al.* 2001). This indentation caused by the electrode of the spot weld machine. All the regions in the FE modeling were connected by sharing nodes. The overlap joint is subjected to a constant velocity of 1 mm/min. The line of action is not initially parallel to the adhesive layer as shown in Fig. 2. As the load increases the overlap area bends. Consequently, the ends of the adhesive layer peel and shear stresses appear. These stresses often induce joint failure.

## 2.2 Boundary Conditions

The boundary conditions associated with each finite element model can be summarized as follows.

On the edges  $X=0$ , clamped boundary conditions are imposed,

$$u_x|_{x=0} = u_y|_{x=0} = u_z|_{x=0} = 0 \quad (1)$$

Whereas both strips are subjected to a fixed y-direction boundary condition for 30 mm segment of strip A ( $X=0$  to 30 mm) and at the end 30 mm segment of strip B ( $X=145$  to 175 mm).

$$u_y|_{x=0-30} = u_y|_{x=145-175} = 0 \quad (2)$$

In the overlap area, tie constraints are imposed between components of welded joints; *i.e.* strip A, strip B, adhesive layer, and weld nugget. By doing so, the translational and rotational boundary conditions of tied surfaces are made identical, regardless of the way these parts are meshed.

The model is subjected to a constant velocity ( $V=1$  mm / min.) at the right edges of strip B.

$$V_x|_{x=175} = 1 \text{ mm / min} \quad (3)$$

## 2.3 Finite Element Mesh

The finite element computation is carried out using ABAQUS software. The finite-element meshes of these models are generated using eight-node-linear brick reduced integration elements. Figure 3 shows the FE meshes for adhesive model (bonded) and weld-bonded models, respectively.

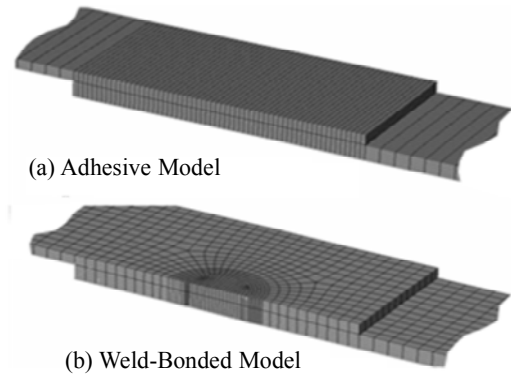


Figure 3. Finite element mesh for both bonded and weld-bonded models

The mesh of bonded model is straight forward and simpler because of the absence of spot welding, which leads to only the overlap area that needs to be divided into fine mesh. However, the spot and weld-bonded models need further fine mesh on the edges of spot weld and adhesive layer to reduce modeling errors. The numbers of elements for the different models, after several trials of refined meshes to ensure the conversion of FE results, are given in Table 1.

## 3. Results

### 3.1 Material Properties

The material properties used throughout the present

work are given in Table 2. These properties were obtained in the laboratory.

**Table 1.** Elements number used in different models

Model	Bonded Model	Spot Model	Weld-Bonded Model
Strip A 1mm	13582	4072	4072
Strip B 1.5mm	20292	6108	6108
Adhesive Layer	1891	---	472
Nugget	----	1140	1254

**Table 2.** Material properties of strip and adhesive

Material	Adhesive	AISI 304 Steel	Brass
Young's Modulus $E$ (GPa)	1.9	193.7	105.33
Possion's Ratio $\nu$	0.37	0.30	0.34
Yield Stress $S_y$ (MPa)	32	277.3	255
Ultimate Stress $S_{ut}$ (MPa)	60.4	729.2	407.5
Melting Point (°C)	63	1464	920

The elastic-plastic properties of the joint are needed for the FE modeling. This requires identifying and determining accurately each region of the spot welded joint, which is achieved by conducting microhardness measurements across the joint specimens. Therefore, Vickers micro-hardness measurements of the weld nugget, HAZ, and base metal of spot welded joints are carried out at a load of 100 gram. The measurements started from the center of the nugget moving outwards step by step to the HAZ then to the base metal, with an incremental distance of 0.25mm.

Spherical indentation (2mm diameter) is used to define the plastic properties of the nugget and heat affected zone for only the AISI 304 steel. This is because steel's properties are affected by the heat. However, brass is not affected by the heat during spot welding process. Consequently, the true stress-true strain curves for AISI 304 steel in these regions are derived using Ahn-Equation:

$$\sigma = \left( \frac{1}{\psi} \right) P_m = \left( \frac{1}{\psi} \right) \left( \frac{P}{\mu a_c^2} \right) \quad (4)$$

$$\varepsilon = \left( \frac{\alpha}{\sqrt{1-(a_c/R)^2}} \right) \left( \frac{a_c}{R} \right) \quad (5)$$

where  $\sigma$  is the true stress,  $\psi$  is an empirical factor which is equal to 3.6.  $P$  is the load,  $P_m$  is the mean pressure,  $a_c$  is the contact radius between the indenter and the material,  $\varepsilon$  is the true strain,  $\alpha$  is the adjustment constant taken as 0.14 (Jeon *et al.* 2006), and  $R$  is the indenter radius. The true stress-true strain curves of the base metal, HAZ, and nugget of spot welded joint for AISI 304 steel are shown in Fig. 4. For the brass, being not affected by heat, the true stress-true strain curves is the same for base metal, HAZ, and nugget of spot welded joint as shown in Fig. 5.

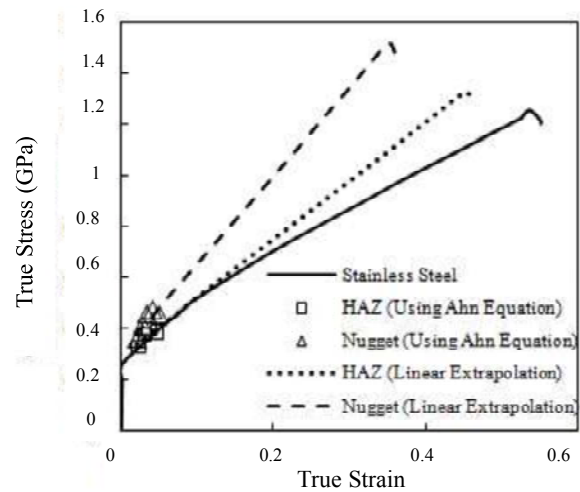


**Figure 4.** True stress-true strain curves of the base metal, HAZ, and nugget of spot welded joint for AISI 304 steel

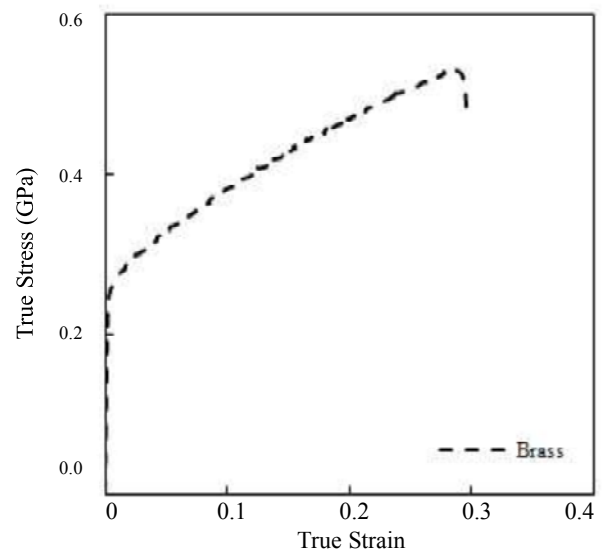


**Figure 5.** True stress-true strain curves for brass

In order to ensure the micro-hardness results, a micro structure of welding cross section was consid-

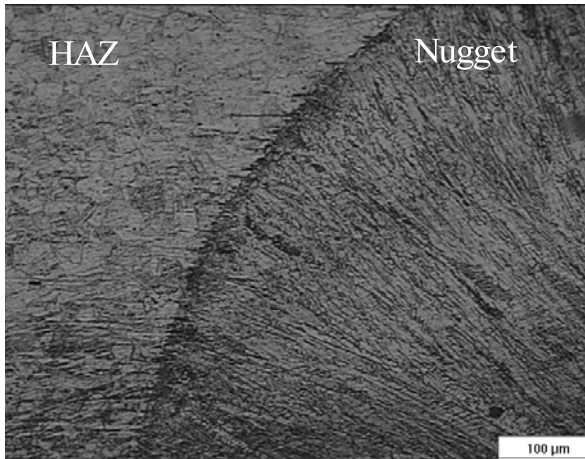


**Figure 6.** Micro structure of nugget and HAZ for AISI 304 steel

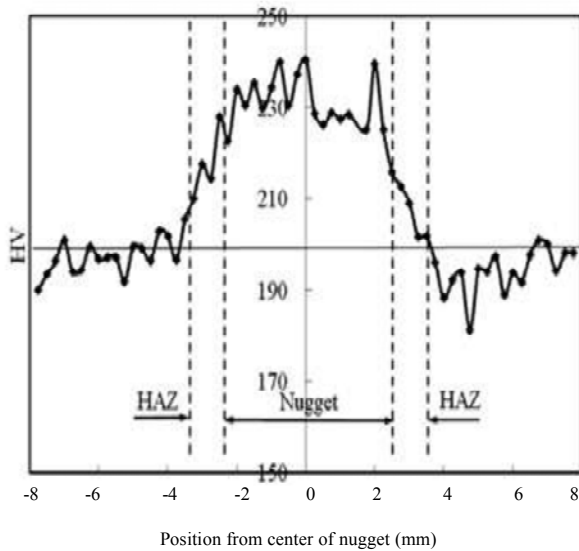


**Figure 7.** Micro-hardness vickers test results for AISI 304 steel

ered. After grinding and polishing, the specimen was etched by dipping into a solution of 10 ml nitric acid, 10ml acetic acid, 5ml glycerin and 15 ml hydrochloric acid, followed by washing in stream of water. Finally, the micro structure was examined for AISI 304 steel using optical microscope as shown in Fig. 6. The micro structure of brass is not changed during the process of spot welding which leads to constant hardness for base metal, HAZ, and nugget areas.

The results of micro-hardness testing for AISI 304 steel are plotted in Fig. 7. It is clear from the figure that the nugget has the highest hardness, followed by the HAZ, and finally the base metal. In addition, the dimension of each region is described clearly in the figure.

To obtain the fracture initiation point (maximum load) as one of the results of finite element modeling, the fracture initiation limits have to be introduced in the model. These properties can be defined and evaluated from the notch tensile test. In ABAQUS software,

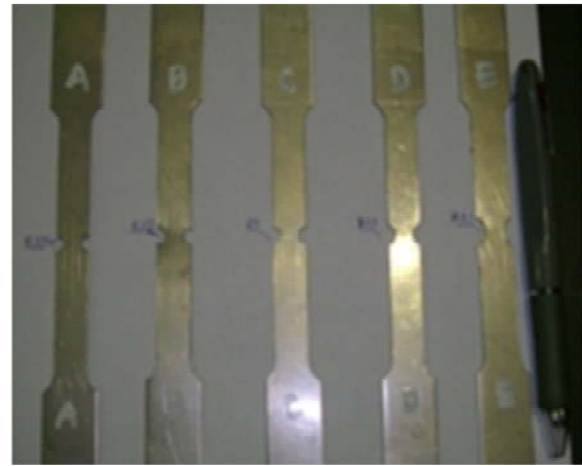


**Figure 8.** Notched brass specimens prepared for tensile test

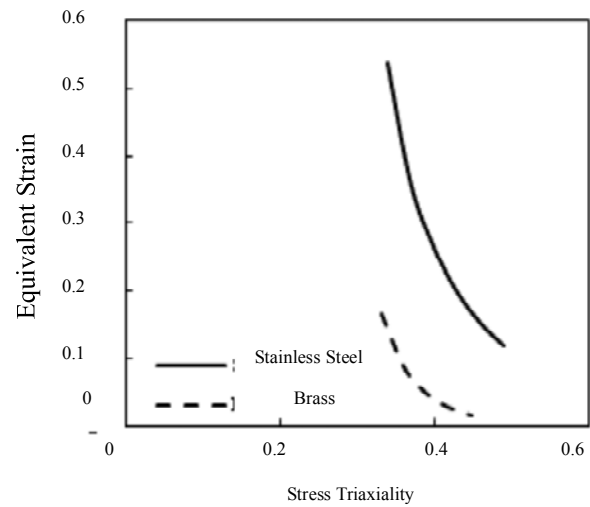


**Figure 9.** The ductile fracture limit properties

the ductile fracture limits are defined in terms of stress triaxiality and corresponding equivalent fracture strain. The basic theories of the stress triaxiality are described in references (Bao 2005; Mackenzie *et al.* 1977; Hancock, Mackenzie 1976).

Mackenzie *et al.* (1977) defined the stress triaxiality for cylindrical specimen as:

$$\sigma_{Triaxiality} = \sigma_m / \sigma' \quad (5)$$

where  $\sigma_m$  is the mean principal stress, and it is defined as:

$$\sigma_m = (\sigma_1 + \sigma_2 + \sigma_3) / 3 \quad (6)$$

and  $\sigma'$  is the effective stress which is defined as:

$$\sigma' = [1/2\{(\sigma_1 - \sigma_2)^2 + (\sigma_2 - \sigma_3)^2 + (\sigma_3 - \sigma_1)^2\}]^{1/2} \quad (7)$$

where  $\sigma_1$ ,  $\sigma_2$ , and  $\sigma_3$  are the principal stresses.

In order to obtain the stress triaxiality and its corresponding equivalent fracture strain values for sheet specimen, notch tensile specimens were prepared and tested according to the standard tensile test. Five notch specimens were prepared with notch radii of 2, 2.5, 3, 4, and 5.1mm, respectively, for each material. Figure 8 shows a picture of notched brass specimens before subjected to tensile test.

Standard tensile tests were conducted on each samples as stated above, a complete load displacement curve is obtained from the tests. The equivalent true strains at the fracture initiation were calculated automatically using the Bluehill-software. Then, the stress triaxiality at the determined equivalent strain was calculated numerically using ABAQUS software.

The stress triaxiality values and the corresponding equivalent fracture strains for AISI 304 steel and brass are plotted in the Fig. 9. The data were extrapolated as an exponential curve, based on a recommendation of previous researchers (Bao 2005; Mackenzie *et al.* 1977; Hancock, Mackenzie 1976).

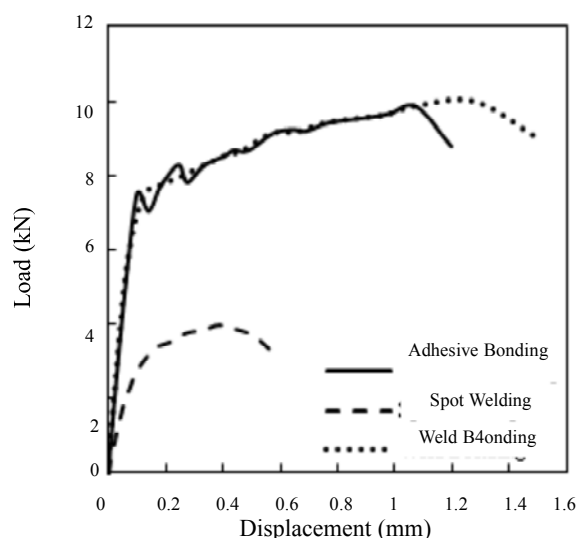
The adhesive layer model is developed based on traction separation mode. After defining all materials properties, the FE models are run to obtain the load-displacement curves.

### 3.2 Finite Element Results

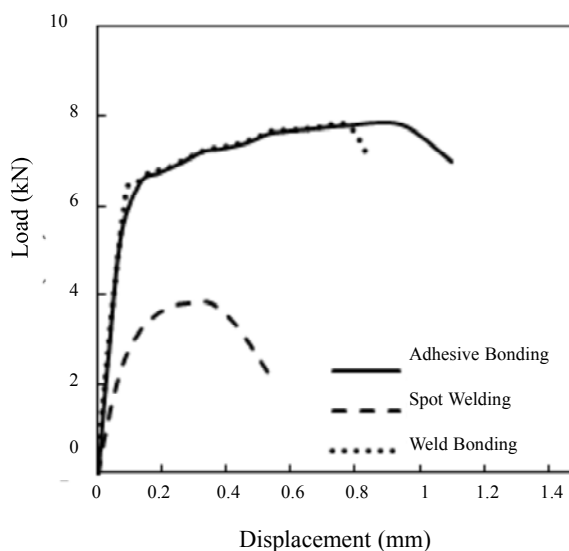
In this section, the results of the finite element simulations for bonded, spot weld, and weld-bonded dissimilar materials and thickness joints are examined. The combination dissimilar materials used in the analysis are steel-brass. In the first combination, the material for strip A is steel with 1mm thickness while the material for strip B is brass with 1.5 mm thickness. In the second combination, strip A represents steel with 1.5 mm thickness while strip B represents brass with 1mm thickness.

Figure 10 shows three different load-displacement curves for joining steel (1 mm thickness) with brass (1.5 mm thickness). When both materials are joined by spot weld, the joint can withstand a maximum load of 4 kN at a displacement of 0.39 mm. When they are joined by adhesive, the load reaches 9.9 kN and the displacement reaches 1.08 mm. Adding an adhesive layer to the spot weld, the maximum load is slightly increased to 10 kN and the displacement is increased to 1.28 mm.

Figure 11 shows three different load-displacement curves for joining steel (1.5 mm thickness) with brass (1mm thickness). When the materials are joined by spot weld, the joint can hold up to a maximum load of 3.8 kN at a displacement of 0.29 mm. When they are joined by adhesive, the load reaches 7.79 kN and the displacement reaches 0.94 mm. Adding an adhesive layer to the spot weld, the maximum load is almost the



**Figure 10.** Load displacement curves for joining steel (1 mm thickness) with brass (1.5 mm thickness)



**Figure 11.** Load displacement curves for joining steel (1.5 mm thickness) with brass (1 mm thickness)

same at 7.78 kN. However, the displacement is reduced to 0.78 mm.

Figure 11. Load displacement curves for joining steel (1.5 mm thickness) with brass (1 mm thickness) The maximum load ( $P$  kN) and corresponding displacement ( $\delta$  mm) obtained from both Figs. 10 and 11 can be summarized in Table 3. The results show that when the thinner strip is steel, the weld-bonded model can withstand larger load and longer extension. In case the thinner strip is brass, both bonded and weld-bonded models have almost the same maximum load, however, bonded model has longer extension.

**Table 3.** Maximum load-displacement for different models combinations

Model Combination	Spot		Bonded		Weld-Bonded	
	P kN	$\delta$ mm	P kN	$\delta$ mm	P kN	$\delta$ mm
Steel 1.0 mm	4	0.39	9.9	1.08	10	1.28
Brass 1.5 mm						
Steel 1.5 mm	3.8	0.29	7.79	0.94	7.78	0.78
Brass 1.0 mm						

## Conclusions

A three-dimensional finite element model for dissimilar materials and thickness are developed. This includes the 3-D finite element modeling of the spot welded, bonded and weld-bonded joints under axial loading conditions. The combinations of dissimilar materials that are used in the analysis are steel-brass. In the first combination, steel is thinner than brass while in the other combination, the brass is thinner than the steel. For each combination, the load-displacement curves for all three joining types are successfully obtained.

When the thinner strip is steel, the bonded model is 2.47 times better than spot model in terms of load carrying capacity. Adding the adhesive layer to the spot model will result in a very small improvement in maximum load bearing capacity. However, the displacement is improved by 15.63%. When the thinner strip is brass, both bonded and weld-bonded models have almost the same maximum load, however, it is better to use the bonded model because the displacement in bonded is more than the weld-bonded by 20.5%. In general, for a model with dissimilar materials and thickness, it is better to use the weld-bonded model when the strip of the softer material has the large thickness and to use the bonded model when the strip of the harder material is thick.

## Acknowledgments

The author is grateful for the College of Engineering Research Center at King Saud University, for the support of this work (Project No. 19/428).

## References

Al-Bahkali E, Es-Saheb M, Herwan J (2010), Finite element modeling of weld-bonded joint. The 4<sup>th</sup> Int. Conf. on Advanced Computational Engineering and Experimenting, Paris, France.

- Bao Y (2005), Dependence of ductile crack formation in tensile tests on stress triaxiality stress and strain ratios. *J. of Engineering Fracture Mechanics* 72: 502-522.
- Baohua C, Yaowu S, Liangqing L (2001), Studies on the stress distribution and fatigue behavior of weld-bonded lap shear joints. *J. of Materials Processing Technology* 108:307-313.
- Bouyousfi B, Sahraoui T, Guessasma S, Chaoch K (2007), Effect of process parameter on the physical characteristic of spot weld joints. *J. of Materials and Design* 28:414-419.
- Cavalli M, Thouless M, Yang Q (2004), Cohesive-zone modeling of the deformation and fracture of weld-bonded joints. *Welding Journal* 133-139.
- Dao M, Chollacoop N, Van Vliet KJ, Venkatesh TA, Suresh S (2001), Computational modeling of forward and reverse problems in instrumented sharp indentation. *Acta Materialia* 49:3899-3918.
- Darwish S (2004), Analysis of weld-bonded dissimilar materials. *Int. J. of Adhesion and Adhesives* 24: 347-354.
- Diehl T (2005), Modeling surface-bonded structures with ABAQUS cohesive elements: beam-type solution. *ABAQUS User's Conference*.
- Furukawa K, Katoh M, Nishio K, Yamaguchi T (2006), Influence of electrode pressure and welding conditions on the maximum tensile shear load. *Q, J. of the Japan Welding Society* 10-16.
- Hancock JW, Mackenzie AC (1976), On the mechanism of ductile failure in high-strength steels subjected to multi-axial stress-states. *J. of the Mechanics and Physics of Solids* 24:147-169.
- Hasanbasoglu A, Kacar R (2007), Resistance spot welding of dissimilar materials (AISI 316L-DIN EN 10130-99). *J. of Materials and Design* 28:1794-1800.
- Jeon E, Kim JY, Baik MK, Kim SH, Park JS, Kwon D (2006), Optimum definition of true strain beneath a spherical indenter for deriving indentation flow curves. *J. of Materials Science and Engineering A* 419:196-201.
- Kang BSJ, Yao Z, Barbero EJ (2006), Post-yielding stress-strain determination using spherical indentation. *Mechanics of Advanced Materials and Structures* 13(2):129-138.
- Kong X, Yang Q, Li B, Rothwell G, English R, Ren H (2008), Numerical study of spot-welded joints of steel. *J. of Materials and Design* 29:1554-1561.
- Li S, Thouless MD, Waas AM, Schroeder JA, Zavattieri PD (2005), Use of mode I cohesive zone models to describe the fracture of an adhesively-bonded polymer-matrix composite. *J. of Composite Science and Technology* 65:281-293.
- Li S, Thouless MD, Waas A.M, Schroeder JA, Zavattieri PD (2006), Mixed-mode cohesive-zone

- models for fracture of an adhesively bonded polymer-matrix composite. *J. of Engineering Fracture Mechanics* 73:64-78.
- Mackenzie AC, Hancock JW, Brown DK (1977), On the influence of state of stress on ductile failure Initiation in high strength steels. *J. of engineering fracture mechanics* 9:167-188.
- Sun C, Thouless MD, Waas AM, Schroeder J, Zavattieri PD (2009), Rate effects for mixed-mode fracture of plastically-deforming adhesively-bonded structures. *Int. J. of Adhesion and Adhesives* 29:434-443.
- Venkatesh TA, Van Vliet KJ, Giannakopoulos AE, Suresh S (2000), Determination of elasto-plastic properties by instrumented sharp indentation: guidelines for property extraction. *Scripta Materialia* 42:833-839.
- Yang QD, Thouless MD, Ward SM (2001), Elastic-plastic mode II fracture of adhesive joints. *International Journal of Solid Structure* 38:3251-3262.